International Journal on Magnetic Particle Imaging
Vol 10, No 1, Article ID 2411002, 12 Pages

Infinite Science Publishing

Research Article

Dynamic image reconstruction in MPI with RESESOP-Kaczmarz

Marius Nitzsche* · Bernadette N Hahn

Department of Mathematics, University of Stuttgart, Germany
*Corresponding author, email: marius.nitzsche@imng.uni-stuttgart.de

Received 25 January 2024; Accepted 24 July 2024; Published online 22 November 2024

Abstract

In Magnetic Particle Imaging (MPI), it is typically assumed that the studied specimen is stationary during the data acquisition. In practical applications however, the searched-for 3D distribution of the magnetic nanoparticles might show a dynamic behavior, caused by e.g. breathing or movement of the blood. Neglecting those dynamics during the reconstruction step results in motion artifacts and a reduced image quality. This article addresses the challenge of capturing high quality images in the presence of motion. A promising technique provides the Regularized Sequential Subspace Optimization (RESESOP) algorithm, which takes dynamics as model inexactness into account, significantly improving reconstruction compared to standard static algorithms like regularized Kaczmarz. Notably, this algorithm operates with minimal prior information and the method allows for subframe reconstruction, making it suitable for scenarios with rapid particle movement. The performance of the proposed method is demonstrated on both simulated and real data sets.

I. Introduction

Magnetic Particle Imaging (MPI), initially proposed by Gleich and Weizenecker [1], is an emerging imaging modality that enables insights into a specimen by measuring the response of superparamagnetic nanoparticles to an applied magnetic field. To this end particles are injected with a certain tracer concentration $c : \Omega \mapsto \mathbb{R}_+ \cup 0$ into the area of interest, which is called the field of view $\Omega \subset \mathbb{R}^3$. Through layering two magnetic fields, i.e. the drive field and the selection field, a field-free point moves through the field of view along a Lissajous trajectory. The time interval of one Lissajous trajectory is called *frame*. The dynamic field excitation caused by the moving field-free point results in a time-varying magnetization M of the injected particles, which induces a measurable voltage v^P over a time interval $I := [0, \mathrm{T}]$ in the receive coils. To reconstruct c it is necessary to separate it from M by $M = c\,\bar{m}$ with the particles' mean magnetic moment $\bar{m} : \Omega \times I \mapsto \mathbb{R}^3$. Knowing this, at the core of MPI lies the fundamental equation

$$v^P(t) = \int_\Omega c(x) \underbrace{(-a * \mu_0 p^R(x)^T \frac{\partial}{\partial t} \bar{m}(x,t))}_{=:S(x,t)} \mathrm{d}x, \; t \in I \quad (1)$$

where μ_0 is the constant magnetic permeability of vacuum and $p^R : \Omega \mapsto \mathbb{R}^3$ is the receive coil sensitivity. The analog filter $a : [-\mathrm{T}, \mathrm{T}] \to \mathbb{R}$ is applied to mitigate the direct feedthrough, a voltage induced by the applied magnetic field.

In MPI, two key challenges arise. The determination of $\bar{m}(x,t)$ from given tupels (c, v^P) is called the *calibration problem*. The standard procedure relies on a time consuming measurement-based approach [2]. Alternatively, model-based techniques are explored which offer a less resource-intensive path, although they may not deliver the same level of precision, see e.g. [3]. A first step to

compensate for such inexactnesses of the resulting system matrix within the reconstruction step was proposed in [4].

In this research, our primary focus is on the *image reconstruction problem*. In other words, the goal is to determine the tracer concentration $c(x)$, $x \in \Omega$ from observed measurements $v^P(t)$, $t \in I$ with a given system function. This process necessitates the discretization of (1), yielding a linear system

$$Ac = v, \quad A \in \mathbb{R}^{N \times M}, c \in \mathbb{R}^M, v \in \mathbb{R}^N, \tag{2}$$

with given system matrix A, measurement vector v and searched-for discrete concentration c. The dimensions are given by N, which is the number of considered temporal points multiplied by the number of receive coils being usually three, as well as the number of spatial points M of the discretized field of view.

The most common solver in MPI is the Kaczmarz method with Tikhonov regularization, also called regularized Kaczmarz, which mainly consists of a fixed point iteration. By iteratively projecting the approximate solution orthogonally onto affine subspaces, the method solves the linear system in (1). More insights can be found in the literature, see e.g. [2].

I.I. Dynamics in MPI

The regularized Kaczmarz method works well if the searched-for concentration is stationary. Be that as it may, many potential clinical applications rely on the reconstruction from dynamic MPI data, e.g. imaging blood flow [5], tracking medical instruments [6] or monitoring of strokes [7, 8]. If the concentration is time-dependent and changes during the data acquisition, motion artifacts will arise in the reconstructions unless the dynamics are compensated for within the reconstruction step. This issue is exacerbated in the so-called multi-frame scenario, where the concentration is reconstructed from multiple data sets that are blockwise averaged over time to improve the signal-to-noise ratio and the spatial resolution of the image.

The regularized Kaczmarz method does not take dynamics of the concentration into account. Figure 1 illustrates motion artifacts arising in single- as well as multi-frame reconstructions. As example, we considered simulated noise free data for a fast rotating cylinder, more precisely it performs one full rotation during the acquisition of seven frames. Information about the simulation settings is detailed in Section III. A 2D slice of the 3D ground truth at time instance $t = 0$ is depicted in subfigure (a). Reconstruction results from a single-frame data set with regularized Kaczmarz are shown in subfigures (c) and (d) for different regularization parameters λ with the one in (d) being optimal with respect to producing minimal visual motion artifacts. In both cases, the computed solution is not sharp and includes motion artifacts. Even

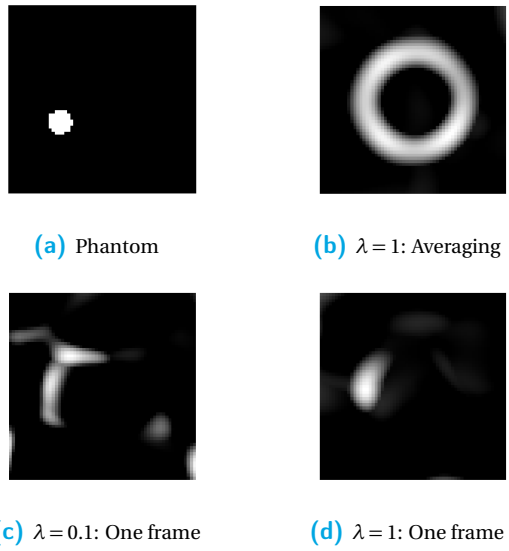

(a) Phantom **(b)** $\lambda = 1$: Averaging

(c) $\lambda = 0.1$: One frame **(d)** $\lambda = 1$: One frame

Figure 1: Reconstruction results with regularized Kaczmarz from noise free data of a fast rotating cylinder.

with the optimal parameter the method is not able to provide a good approximation to the ground truth while the averaging of 20 frames in the multi-frame scenario further increases the motion artifacts, see subfigure (b).

Consequently, it becomes imperative to account for dynamics, i.e. to address the image reconstruction task as a dynamic inverse problem. A universal, standardized regularization technique for dynamic inverse problems does not exist. While a multitude of approaches have been proposed for individual traditional tomographic applications, only a few have been presented in the field of MPI in response to this challenge.

For instance, a strategy to account for periodic motion by pre-processing the measured data is developed in [9]. By estimating the motion frequency associated with periodic motion, the authors effectively grouped data samples and thus generated static single-frame data sets for the individual states of the object. Consequently, an image of each state can be reconstructed with standard static algorithms. This approach has also been extended to multi-patch MPI [10].

A dynamic forward model within MPI is offered in [11], which is combined with a reconstruction method using temporal splines to increase temporal resolution in [12].

Another approach is based on estimating the motion using optical flow, a computationally expensive method that has been examined in applications like CT or MRI [13]. Its application in a dynamic MPI scenario was first proposed in [14] and in more detail in [15] using a stochastic primal-dual algorithm to jointly estimate the motion and reconstruct the image.

10.18416/ijmpi.2024.2411002

In this article we propose to apply the Regularized Sequential Subspace Optimization method (RESESOP) for inexact model operators [16] to the dynamic MPI problem. With this method we take motion implicitly as model inexactness into account and are able to reconstruct images from motion corrupted data, which are of higher quality than those computed by regularized Kaczmarz, without the need of explicitly estimating the motion. We will see that the only required a priori information can be gained from the measured MPI data itself. Furthermore, no special pre-processing of the data beyond the standard is required.

The article is organized as follows. In Section II we first introduce the mathematical model of time-dependent concentration reconstruction in MPI and argue that dynamics induce model inexactness. We then present the general concept of the RESESOP and transfer it to the dynamic reconstruction problem in MPI. In particular, we discuss how the required a priori information on the model inexactness can be extracted directly from the measured MPI data. Finally, we provide a detailed numerical evaluation of the method. The respective test cases, including simulated as well as real data sets, are introduced in Section III. In Section IV, we present respective reconstruction results and analyze the performance of the proposed algorithm.

II. Methods

As illustrated in the introduction, reconstruction algorithms need to account for dynamics of the studied concentration. In order to develop such algorithms, the time-dependency of the concentration first needs to be incorporated into the mathematical model of MPI, i.e. in equation (1) and (2), respectively.

II.I. The mathematical model of MPI with time-dependent concentrations

Imaging a time-dependent particle concentration, i.e. $c : \Omega \times I \mapsto \mathbb{R}_+ \cup 0$, implies that it is changing during the measuring process. In the most extreme scenario, the time-scale of the concentration dynamics coincides with the one of the data acquisition, i.e.

$$v^P(t) = \int_\Omega c(x,t) S(x,t) \mathrm{d}x, \quad t \in I \tag{3}$$

or in the discretized setting

$$A_t c_t = v_t \quad \forall\, t \in [0,T],\ A_t \in \mathbb{R}^{3\times M},\ c_t \in \mathbb{R}^M,\ v_t \in \mathbb{R}^3. \tag{4}$$

In other words, each single measure $v^P(t)$ (respectively v_t), t being one particular time instance, captures a different state of the concentration. Even with strong a priori assumptions a dynamic concentration reconstruction on the same temporal granularity as defined by the sampling rate of the measurement process is hardly possible.

However, an important characteristic of MPI are the very fast measurement times which imply that the temporal resolution of the concentration is typically several orders coarser than the data sampling rate. Thus, it is reasonable to assume that the searched-for concentration is piecewise constant in time. This motivates to formally split the time interval I into N_τ pairwise disjoint time subintervals $I_i := [\tau_i, \tau_{i+1})$ with $i = 0, 1, \ldots, N_\tau - 1$ as well as $\tau_0 := 0$ and $\tau_{N_\tau} := T$. As a consequence it holds

$$I = \dot{\cup}_{i=0,1,\ldots,N_\tau-1} I_i, \quad c(x,t) = c_{\tau_i}(x) \text{ for } t \in I_i.$$

Both the time scale of the measurement and the coarser time scale of the dynamic concentration can then be coupled by a function

$$\gamma : I \to \{\tau_i,\ i = 0,1,\ldots,N_\tau - 1\},\ \gamma(t) := \tau_i \text{ if } t \in I_i.$$

With this notation, the general dynamic reconstruction problem can be formulated as

$$v^P(t) = \int_\Omega c(x,\gamma(t)) S(x,t) \mathrm{d}x, \quad t \in I, \tag{5}$$

or in discretized form

$$A_i c_{\tau_i} = v_i \quad \forall\ i \in \{0,1,\ldots,N_\tau - 1\} \tag{6}$$

with given $A_i \in \mathbb{R}^{(N_i\cdot 3)\times M}$, searched-for $c_{\tau_i} \in \mathbb{R}^M$ and measured $v_i \in \mathbb{R}^{(N_i\cdot 3)}$, where N_i denotes the number of time samples per sub-interval I_i.

In Section II.II, we will focus on solving the discretized dynamic inverse problem. Considering each *subproblem* $A_i c_{\tau_i} = v_i$ individually would formally allow the application of a classic static reconstruction method. However, in analogy to the multi-frame approach, the goal is to improve the SNR and the spatial resolution of the images. In order to achieve this in the presence of motion, correlations between the states have to be exploited within the joint reconstruction step. Furthermore, if the length of a subinterval I_i is smaller than the time required to measure one complete frame, the solution of the respective subproblem has to deal with a limited-data problem.

The actual decomposition of I into subintervals will depend on the specific application. Suitable choices are discussed in the following subsection.

II.I.1. Choosing suitable subintervals

In the multi-frame scenario, an intuitive idea is to let each subproblem coincide with one frame. Indeed, many concentration dynamics might be assumed stationary within one frame. The actual time to acquire data for one frame is very small, e.g. for a 3D field of view, it takes 21.54 ms. Thus, for velocities lower than 10 centimeters per second, for instance, the travelled distance within the

21.54 ms is smaller than the length of the edge of a voxel [17]. Additionally, the usage of frames as subproblems simplifies the implementation within an MPI framework. Real data are usually pre-processed and stored frame-by-frame. Thus, a dynamic reconstruction algorithm working on frames can be embedded directly in existing MPI software pipelines.

However, if the examined structure changes faster than the acquisition of one frame, e.g. due to a pulsating motion or a fast rotation, this rigid coupling of time scales is not feasible and would still lead to motion artifacts. A way to handle these scenarios is to choose smaller subproblems which are then even more underdetermined than the original inverse problem. Looking at it from a practical perspective, one timestep t is equivalent to 0.8μs in MPI. Thus, choosing subproblems corresponding to either one frame, half a frame or a quarter of a frame seem adequate to represent and capture most relevant concentration dynamics.

II.I.2. Interpreting the dynamics as model inexactness

A common strategy in dynamic imaging problems is the incorporation of motion models to relate the different states of the object to each other, see e.g. [18, 19]. In our case, this means that instead of considering a series of independent concentrations c_{τ_i}, it is assumed that they are all linked together by an underlying motion model Γ, for instance

$$c(x,t) = c_0(\Gamma_t(x))$$

with a reference configuration c_0, e.g. the concentration $c_0 = c(\cdot,0)$ at the initial time of the data acquisition. Incorporating such a motion model into the equation (5) and using an appropriate change of coordinates yields an inverse problem for the reference concentration c_0 with a forward operator depending on the motion information Γ, i.e. in the discretized setting

$$A_{i,\Gamma} c_0 = v_i \quad \forall\, i \in \{0,1,\dots,N_\tau - 1\} \tag{7}$$

with $A_{i,\Gamma} \in \mathbb{R}^{(N_i \cdot 3)\times M}$. Please note that we use the same symbol c_0 in both continuous and discretized setting for the reference configuration in order to keep the notation as simple as possible. A detailed derivation in the general context of inverse problems can be found in [18]. Thus, extracting the time-dependent concentrations $c(\cdot,t)$ is equivalent to extracting the motion information Γ and the reference concentration c_0.

In general, the exact motion Γ will be unknown, i.e. in practice, one can only use an approximate forward operator to determine c_0, e.g. the static model A_i if no further information on the dynamics are available. Therefore, we treat the dynamics in the following as inexactness in the forward model and account for this inexactness while recovering c_0 from the measured dynamic data v_i, $i = 0,1,\dots,N_\tau - 1$.

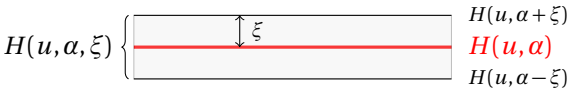

Figure 2: Illustration of a stripe

II.II. RESESOP method for solving inverse problems with inexact forward operator

In this work we propose to solve the dynamic reconstruction problem in MPI (7) with the RESESOP-Kaczmarz method developed in [16] for solving general inverse problems with inexact forward operator.

This method is based on the Sequential Subspace Optimization method (SESOP) [20]. It is an iterative method that approximates the searched-for solution f of a given linear inverse problem $Bf = g$ by the following scheme: In the n-th step, compute

$$f_{(n+1)} = P_H(f_{(n)})$$

with the metric projection P_H onto an intersection $H = \cap_{j\in J_n} H(u_j,\alpha_j)$ with hyperplanes

$$H(u,\alpha) = \{x \in X : \langle u,x\rangle = \alpha\}.$$

In particular, each iteration has the following choices of freedom:

- a finite index set J_n with $|J_n|$ denoting the number of search directions u_j and thus the number of hyperplanes used in the n-th iteration,
- search-directions u_j and parameters α_j which are chosen in accordance to the right-hand side g and the forward model B, for instance, in case $J_n = \{n\}$ a suitable choice is $u_n = B^*(Bf_{(n)} - g)$ as well as $\alpha_n = \langle Bf_{(n)} - g, g\rangle$.

This method relies on knowing the exact forward model B and on exactly known right-hand side g. In practice however, only noisy data g^δ with noise level $\|g - g^\delta\| \le \delta$ can be measured and, as in our case, only an inexact forward operator B^η with inexactness level $\|B - B^\eta\| \le \eta$ might be available for the reconstruction. Thus, the idea of RESESOP (regularized SESOP) is to replace the hyperplanes $H(u,\alpha)$ by stripes

$$H(u,\alpha,\xi) := \{x \in X : |\langle u,x\rangle - \alpha| \le \xi\},$$

whose width ξ is chosen in dependence on the noise and inexactness levels δ and η, see Figure 2 for an illustration. This idea was originally suggested in [21] for the noisy data case and was expanded to model imperfections in [16]. The introduction of Morozov's discrepancy principle offers a stopping criterion; as a result, it can be proven under certain conditions on the choice of J_n, u_i, α_i, that the method provides a regularized solution to the original inverse problem [21].

10.18416/ijmpi.2024.2411002

Algorithm 1 RESESOP-Kaczmarz

Choose initial guess $c_{(0)}$ and constant $\rho > 0$.
Let $n = 0$ be the iteration index.
Let $n_{\text{full}} = 1$ be the index for full iterations.
while $n < n_{\text{full}} \cdot N_\tau$ **do**
  Check discrepancy principle
  if $\|A_{[n]} c_{(n)} - v_{[n]}^{\eta,\delta}\| \le 1.001 \cdot (\eta_{[n]}\rho + \delta_{[n]})$ **then**
    $c_{(n+1)} = c_{(n)}$
  else
    Choose a finite index set $J_n \subset \{0, 1, \dots, [n]\}$
    Choose search directions $u_{n,j}$ for all $j \in J_n$
    Define $H_{(n)}^{\eta,\delta} := \bigcap_{j \in J_n} H(u_{n,j}, \alpha_{n,j}, \xi_{n,j})$
    with parameters $\alpha_{n,j} = \langle u_{n,j}, c_{(n)} \rangle$
    and $\xi_{n,j} = (\eta_j \rho + \delta_j)\|A_j c_{(n)} - v_j^{\eta,\delta}\|$
    Compute $c_{(n+1)} = P_{H_{(n)}^{\eta,\delta}}(c_{(n)})$
    Update iteration index $n = n + 1$
  end if
end while
if $c_{(n)} \neq c_{(n-N_\tau)}$ **then**
  $n_{\text{full}} = n_{\text{full}} + 1$
  Repeat While Loop
else
  Break
end if

When solving an inverse problem that shows a subproblem structure like (7), it is beneficial to include individual inexactness and noise levels η_i, δ_i, in our case

$$\|v_i - v_i^\delta\| \le \delta_i, \quad \|A_i - A_i^\eta\| \le \eta_i, \quad i \in \{0, 1, \dots, N_\tau - 1\}.$$

In particular, with such estimates, we obtain

$$\|A_i^\eta c - v_i^\delta\| \le \eta_i \rho + \delta_i$$

as upper bound for the residual on the set of solutions whose norm is bounded by $\rho > 0$. For this case, Blanke et al. proposed the so-called RESESOP-Kaczmarz method: Each iteration corresponds to a RESESOP iteration with subproblem specific inexactness and noise levels applied to every subproblem that does not yet satisfy the discrepancy principle. In this way, the algorithm combines all subproblems and incorporates information from all time intervalls I_i simultaneously.

A general form of the RESESOP-Kaczmarz method is stated in Algorithm 1. With n being the current iteration index, the notation $[n] := n \bmod N_\tau$ identifies the corresponding subproblem (6). One full iteration consists of N_τ subiterations, each including a metric projection onto the intersection of stripes $H_{(n)}^{\eta,\delta}$. After each full RESESOP-Kaczmarz iteration, i.e. $[n] = 0$, it is checked, if the discrepancy principle was satisfied for all subproblems.

Algorithm 2 Computation of $P_{H^{\eta,\delta}}(c)$
Example for $|J| = 2$, $J = \{1, 2\}$

Project onto hyperplane $H(u_2, \alpha_2 + \xi_2)$, i.e. compute
$\tilde{c} = P_{H(u_2,\alpha_2+\xi_2)}(c) = c - \dfrac{\langle u_2, c \rangle - (\alpha_2 + \xi_2)}{\|u_2\|^2} u_2$
Check if $\tilde{c}$ is already part of stripe $H(u_1, \alpha_1, \xi_1)$
if $\tilde{c} \in H(u_1, \alpha_1, \xi_1)$ **then**
  $P_{H^{\eta,\delta}}(c) = \tilde{c}$
else
  Project onto $H(u_2, \alpha_2 + \xi_2) \cap H(u_1, \alpha_1 \pm \xi_1)$,
  i.e. compute
  $T = \dfrac{\langle u_1, \tilde{c} \rangle - (\alpha_1 \pm \xi_1))}{\|u_2\|^2 \|u_1\|^2 - \langle u_2, u_1 \rangle^2}$
  $P_{H^{\eta,\delta}}(c) = \tilde{c} + \langle u_2, u_1 \rangle T - \|u_2\|^2 T$
end if

For the example of two search directions, the metric projection can be computed via Algorithm 2.

RESESOP-Kaczmarz does not require extensive or unrealistic a priori information to solve inverse problems with inexact forward models such as dynamic reconstruction problems. The estimates of the uncertainty levels are the only additional information used compared to standard static approaches. Consequently, when applying the method to dynamic problems, the motion information will be implicitly included in the inexactness levels.

However, a sufficiently good estimate is crucial for the performance of RESESOP. If the estimates are too large the convergence of the method can be fast but it leads to a computed solution with a high error rate. If the levels are estimated too low the noise and the model imperfections might not be compensated for sufficiently resulting in a noisy reconstruction with artifacts. The extreme case, where the levels are set to zero, corresponds to a SESOP-Kaczmarz reconstruction without regularization and accounting for model inexactness, i.e. in particular to a static reconstruction where the Kaczmarz loop results in an averaging of the data.

Next, we discuss further adaptions of this general framework to the application in dynamic MPI, in particular how the required estimates can be obtained and how the search directions can be chosen.

II.III. Application in MPI

II.III.1. Inexactness levels in dynamic MPI

We first discuss how to determine estimates for the noise and inexactness levels. In a static multi-frame setting, the noise levels δ_i can be determined by comparing the data vectors measured per frame.

The inexactness levels depend on the selected model for the reconstruction algorithm. Due to the time consuming process of calibration in real MPI and since we assume no further prior information on the unknown

motion Γ, we propose to use the static system matrix A_i as inexact forward model. Without knowledge of Γ, it is difficult to compute a viable upper bound η_i with $\|A_i - A_{i,\Gamma}\| \leq \eta_i$.

However, if we compare again data sets for different frames in a dynamic scenario, their difference captures noise as well as motion. For this reason, we propose to jointly estimate both uncertainty levels together in form of levels $\zeta_i \in \mathbb{R}$ characterizing the total inexactness of the system, more precisely for each subproblem

$$\zeta_i \approx \eta_i \rho + \delta_i, \quad i \in \{0, 1, \ldots, N_\tau - 1\}.$$

These values are computed by comparing the data v_0 of the initial subproblem with data v_i of the i-th subproblem. If the size of each subproblem corresponds to one frame, it is simply $\zeta_i = \|v_0 - v_i\|$.

However, in case of subframe-sized subproblems, this direct comparison is not possible but requires an additional interpolation step beforehand. Each subproblem corresponds to a number of time points t of a frame. Consequently, the data fragment of the initial subproblem is comparable to the data acquired at the same time points of each frame, e.g. the uncertainty levels between the first subproblem of the first frame and the first subproblem of every other frame can be evaluated. However, to compute an estimate for the uncertainty level of another subproblem of the same frame with the same method is impossible. Therefore, we apply a cubic interpolation between comparable data fragments to acquire uncertainty levels for each subproblem.

An alternative method to estimate the uncertainty levels ζ_i is to make use of preliminary regularized Kaczmarz reconstructions. To quantify the error between Kaczmarz's reconstructions, the mean-squared error MSE is used. However, this approach depends on a priori reconstructions which will typically contain artifacts and thus can result in a low MSE. Thus, an extraction directly from measured data seems favorable.

II.III.2. Choice of search directions

The convergence properties of SESOP, and hence RESESOP-Kaczmarz, depend on the number and choice of the search-directions. On the one hand, a higher number of search directions results in more complex and computationally expensive iterations. On the other hand, the algorithm requires in total less iterations to achieve the desired accuracy. In this work we will focus on two search directions which is a compromise between computational expense for one iteration as well as total number of iterations.

More precisely, we choose in the n-th iteration step the finite index set $J_n = \{n_-, n\}$ with n_- representing the last iteration in which the discrepancy principle did not yet hold. The search directions $u_{n,j}$ with $j \in J_n$ are then chosen as

$$u_{n,n_-} = A^*_{[n_-]}(A_{[n_-]}c_{(n_-)} - v_{[n_-]}),$$
$$u_{n,n} = A^*_{[n]}(A_{[n]}c_{(n)} - v_{[n]}).$$

In particular, this choice meets the criteria formulated in [16] that guarantee the convergence of RESESOP-Kaczmarz to a regularized solution of the underlying dynamic inverse problem.

II.III.3. Non-negativity constraints

In the MPI setting the reconstructed image approximates the concentration c, which is a vector consisting of real, non-negative numbers. Therefore, a non-negativity constraint is a common technique to improve reconstruction algorithms [2]. To that end, after each iteration every negative part is set to zero.

III. Data

Our test cases for the numerical evaluation comprise both real and simulated data, each offering valuable insights into the dynamic reconstruction problem in MPI and the performance of the proposed method. This dual test set strategy allows for a robust evaluation under controlled conditions (simulated data) as well as real-world scenarios (real data).

III.I. Simulated Data

We first conduct a fully simulated numerical experiment. This simulated dataset was generated using the model B3 presented by Kluth, Szwargulski, and Knopp [22].

The goal was to construct a similar setup as the available real data. To that end, the phantom is a cylinder rotating through the field of view. There are two different rotation speeds, depending on the number of frames per rotation (fpr). They are equivalent to 44 and seven fpr or more specifically, e.g. between frame one and two, the concentration is displaced by 0.163 voxels in x-direction and 2.277 voxels in y-direction (44 fpr) respectively 6.024 voxels in x-direction and 12.509 voxels in y-direction (7 fpr). Figure 3 illustrates the underlying rotating motion of the object in the simulated test data case.

The simulated system matrix is derived from dynamic simulations of Néel-type particle magnetization dynamics. Here, the uniaxial particle anisotropy varies with position within the field of view. The anisotropy is minimal at the center but intensifies toward the boundaries. This choice aligns with the assumptions in MPI, where the static component of the applied magnetic field is believed to induce physical rotation of particles and influence their combined anisotropy energy landscape.

The simulated data were generated on a 3D grid of $61 \times 61 \times 5$ pixels, each with a resolution of 0.5 mm. A 2D

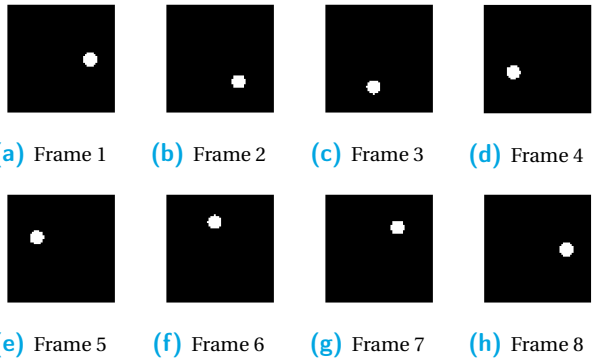

(a) Frame 1 (b) Frame 2 (c) Frame 3 (d) Frame 4

(e) Frame 5 (f) Frame 6 (g) Frame 7 (h) Frame 8

Figure 3: The course of the motion illustrated by the ground truth phantom at the beginning of each trajectory of the fast rotation (seven fpr).

Lissajous excitation was used, with anisotropy constants reaching values as high as 1250 J/m^3. The system matrix was extended to three dimensions by stacking multiple layers in z-direction. In discretized form this resulted in $M = 18605$ spatial points and $N_i = 1633$ temporal points per frame.

To create the system matrix, we utilized a dedicated toolbox presented in Albers, Kluth, and Knopp [23]. To prevent inverse crime, the data were calculated using a slightly shifted, larger matrix, ensuring the integrity of our simulation experiments. Furthermore, we added white Gaussian noise to the data corresponding to a signal-to-noise ratio of 10.

III.II. Real Data

The real data were provided by Brandt from the University of Hamburg and collected by a team at UKE Hamburg led by Knopp. These data encode a glass capillary, which rotates at an average speed of seven Hz and was initially introduced in the study by Gdaniec et al. [9]. This experiment represents a very fast motion.

Working with real data presents some additional challenges compared to simulated data. Typically, one lacks a ground truth which hinders a direct assessment of the accuracy of the reconstruction. Moreover, real measurements usually have high degree of noise, adding complexity to the reconstruction task in the dynamic case where noise levels cannot be reduced by averaging over multiple frames. This is further amplified in MPI due to the fact that the system function is measured as well.

These experiments were conducted using a preclinical MPI scanner from Bruker Biospin in Ettlingen. The imaging setup involved 3D MPI measurements with a Lissajous excitation driven by three sinusoidal drive fields in the x-, y-, and z-directions. These fields operated at frequencies of $f_x = \frac{2.5\text{MHz}}{102}$, $f_y = \frac{2.5\text{MHz}}{96}$, and $f_z = \frac{2.5\text{MHz}}{99}$, with an amplitude of $14\frac{\text{mT}}{\mu_0}$. Each cycle of data acquisition took 21.54 ms, and the induced signal was sampled at intervals of 0.8μs resulting in $N_i = 53857$ temporal points per frame. The measurements covered $M = 15625$ positions in a $25 \times 25 \times 25$ grid. More detailed information can be found in [9].

III.III. Pre-processing

To the real data, the standard pre-processing steps were applied. After applying the Fourier transform, a frequency selection was performed, more precisely all frequencies below 80 kHz and above 625 kHz were eliminated. This was followed by a SNR thresholding. Furthermore, a singular value decompostion as proposed in [24] was performed to reduce the computational cost of reconstructing a three dimensional image. With weigths computed from background measurements, the randomized singular value decomposition trimmed the system matrix to 5000 rows.

However, it is important to note that these conventional pre-processing steps are tailored to full-frame data. Thus, they may encounter limitations when applied to dynamic cases, where the dynamics requires a division of the data into sub-frames. In order to realize this, the raw data first have to be transformed into the time domain with an inverse Fourier transform. Only then the frame-sized problems can be split into smaller subproblems and are consequently solved in time domain. To this end, access to the original raw-data is crucial for the solution of reconstruction problems with fast dynamics. If only pre-processed data are provided, one is restricted to decompositions, where the time intervalls I_i correlate to individual frames.

When working with simulated data, most of the pre-processing steps are not necessary. Due to the 2D-Lissajous excitation, the system matrix is naturally smaller compared to the system matrix of real data. Therefore, pre-processing steps to reduce computational work are not critical and some steps e.g. SNR thresholding not applicable to simulated data.

IV. Results and Discussions

This section is dedicated to the numerical evaluation of the RESESOP-Kaczmarz method on both simulated and real dynamic MPI data. In particular, we investigate the influence of critical parameters of our algorithm on the result.

All experiments are conducted with 3D data, but for clarity, each result is shown with a 2D slice. In each experiment, the same frame and slice are depicted, ensuring a comparable view across all scenarios.

The runtime of the RESESOP-Kaczmarz algorithm is highly dependent on the chosen parameters. In this study, we primarily consider 30 subproblems per iteration, leading to a 2.3 times longer computation time per

Algorithm (**speed**)	PSNR	NRMSE	SSIM
reg. Kaczmarz (**44 fpr**)	22.0459	0.0892	0.8398
RESESOP-K. (**44 fpr**)	23.1104	0.0827	0.8904
reg. Kaczmarz (**7 fpr**)	20.3286	0.0934	0.7346
RESESOP-K. (**7 fpr**)	21.1896	0.0904	0.8266

Table 1: Comparison of reconstructions using regularized Kaczmarz and RESESOP-Kaczmarz of frame four from noisy simulated data with two different rotation speeds.

iteration compared to the regularized Kaczmarz method. However, when using only one subproblem (i.e., solving the problem with RESESOP), the computation time is reduced to 0.2 times that of the regularized Kaczmarz algorithm.

IV.I. Simulated Data

We first present reconstruction results from simulated noisy data, cf. Section III.I, with two different rotation speeds - a very fast scenario of seven fpr as well as the scenario of 44 fpr. Regarding the coupling of time scales, we consider here each frame as one subproblem, i.e. we are choosing the least intrusive version in the MPI pipeline.

To illustrate the motion compensation properties of the RESESOP-Kaczmarz method, we compare the results with those generated by the regularized Kaczmarz-algorithm which is the most commonly used algorithm within MPI. Since averaging data is not recommendable for dynamic data, all reconstructions with regularized Kaczmarz use one frame of data. The method is stopped after 100 iterations. Furthermore, at each iteration non-negativity of the approximated solution is enforced. The initial value was set to zero. The regularization parameter λ is optimized by performing reconstructions for a wide range of parameters and choosing the one that leads to the best result.

The reconstruction results are illustrated in Figure 4. The first row depicts the ground truth at frame four for both rotational velocities. The second row shows the images reconstructed by regularized Kaczmarz. In both dynamic scenarios significant artifacts are visible. Since the algorithm cannot rely on averaging over multiple frames, the noise in the data is not satisfactorily reduced, resulting in artifacts throughout the entire field-of-view. Furthermore, the circular shape of the object is blurred, distorted and hence no more recognizable. As to be expected, this effect is worse the faster the motion. These examples motivate again that the dynamic behaviour of the concentration needs to be taken into account within the reconstruction step.

The respective results of RESESOP-Kaczmarz are presented in the third row of Figure 4. In both dynamic scenarios, the actual shape of the object is recognizable in the reconstructions, i.e. the algorithm does indeed

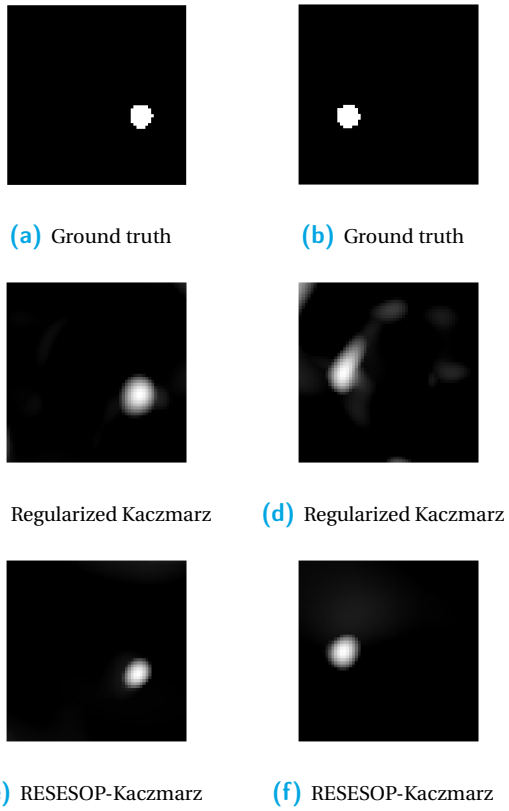

(a) Ground truth **(b)** Ground truth

(c) Regularized Kaczmarz **(d)** Regularized Kaczmarz

(e) RESESOP-Kaczmarz **(f)** RESESOP-Kaczmarz

Figure 4: Dynamic Reconstructions of frame four from noisy simulated data with two different rotation speeds. The left column shows results for a rotation speed of 44 fpr, the right column for seven fpr.

compensate for the motion. However, due to the strict restriction to frame-sized subproblems, we can still observe some small distortions in case of the very fast motion. Also the location of the object is not correctly reconstructed but depicted in the middle of the traveled path during frame four and not in the beginning. However, we further note that in both dynamic cases, the method is able to eliminate the artifacts caused by the noise throughout the field of view.

These findings are supported by comparing the reconstruction results in terms of Peak Signal-to-Noise Ratio (PSNR), Normalized Root Mean Square Error (NRMSE), and Structural Similarity Index Measure (SSIM). The corresponding values for both reconstruction methods and for both slow and fast rotational velocities are provided in Table 1. Reconstructions computed with the RESESOP-Kaczmarz algorithm exhibit higher quality across all metrics, with the improvement being even more pronounced in the fast rotation scenario.

Altogether, Figure 4 and Table 1 demonstrate the advantage of applying RESESOP-Kaczmarz to dynamic MPI problems. Further insights regarding the performance of both algorithms are provided in Figure 5. The plots

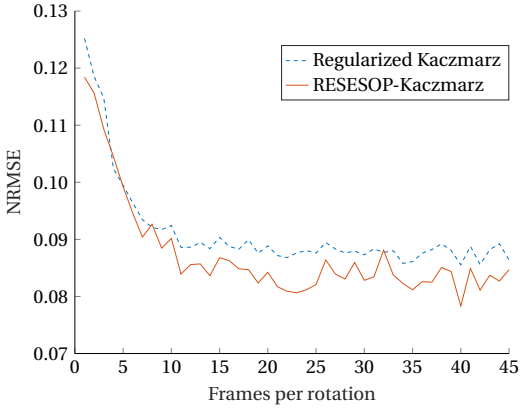

(a) Normalized root mean squared error (NRMSE)

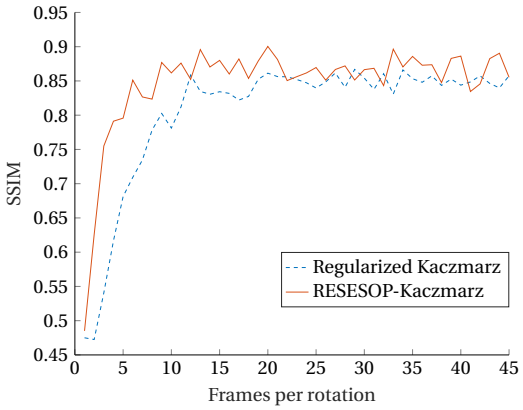

(b) Structural similarity index measure (SSIM)

Figure 5: Comparison of NRMSE and SSIM for reconstruction with regularized Kaczmarz (blue dashed line) and RESESOP-Kaczmarz (orange solid line) in dependence on the rotational speed of the phantom.

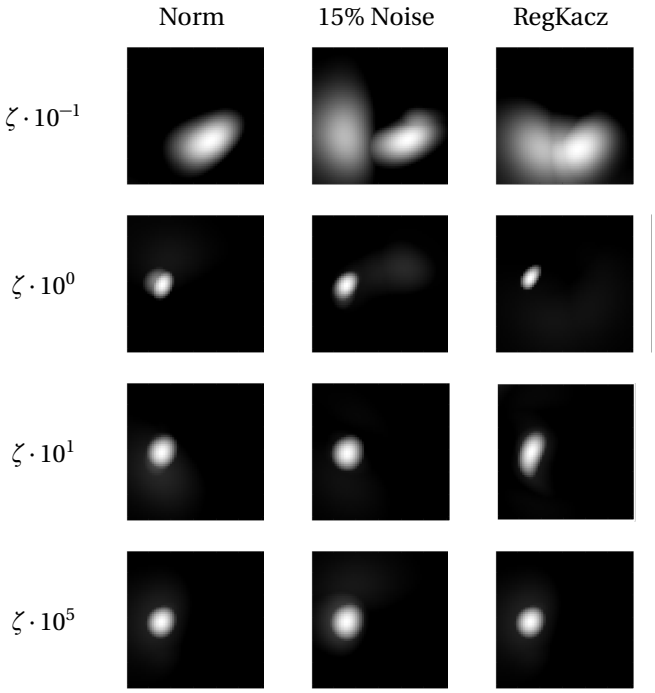

Figure 6: Reconstructed dynamic images with RESESOP-Kaczmarz for different estimates of the total inexactness levels ζ_i. Column 1: computed as distance of two frames via euclidean norm, Column 2 : as in Column 1 with 15 % added noise , Column 3: computed as MSE from regularized Kaczmarz reconstructions. Each row corresponds to one additional scaling factor.

in this figure compare the NRMSE and the SSIM for images reconstructed using the regularized Kaczmarz and RESESOP-Kaczmarz algorithms across different rotational speeds of the phantom. The speed is quantified by fpr, i.e. the smaller the value the faster the motion. Regarding the NRMSE, Figure 5a shows that the proposed RESESOP-Kaczmarz algorithm consistently provides better reconstruction results at all motion speeds. The SSIM further assesses the interpretability of these reconstructions, see Figure 5b. Especially for very fast motion, the RESESOP-Kaczmarz algorithm produces reconstructions of significantly higher quality than the regularized Kaczmarz algorithm. With decreasing speed, the SSIM values then approach each other, however, in average, the RESESOP-Kaczmarz algorithm continues to provide better results with respect to the SSIM.

IV.II. Parameters for RESESOP-Kaczmarz

In this section, we want to study the robustness of the RESESOP-Kaczmarz algorithm regarding estimates of the total inexactness levels ζ_i, number of iterations and size of subproblems. All experiments in this subsection have been conducted with simulated data for the fast rotating object with ten percent of added noise. The reconstruction in Figure 4 (f) was obtained by determining ζ_i as described in Section II.III.1 with the Euclidean norm and by performing ten full RESESOP-Kaczmarz iterations while the size of all subproblems corresponds to one full frame.

To test stability regarding the estimates of the inexactness levels, we performed the reconstruction with scaled versions of these inexactness levels (more precisely with factors 10^{-1}, 10^{1} and 10^{5} respectively) representing an under-, respectively over-estimations. In addition, we also considered testing robustness with respect to computation errors in the uncertainty level estimation. Accordingly, we added normally distributed random numbers multiplied by 15% of the maximum uncertainty level to the norm estimates ζ_i. Lastly, we further use the alter-

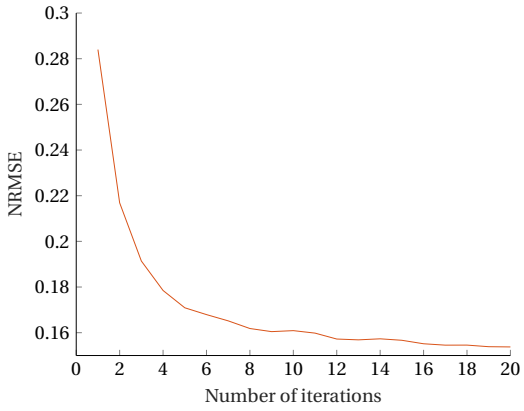

Figure 7: NRMSE in dependence on the number of RESESOP-Kaczmarz loops.

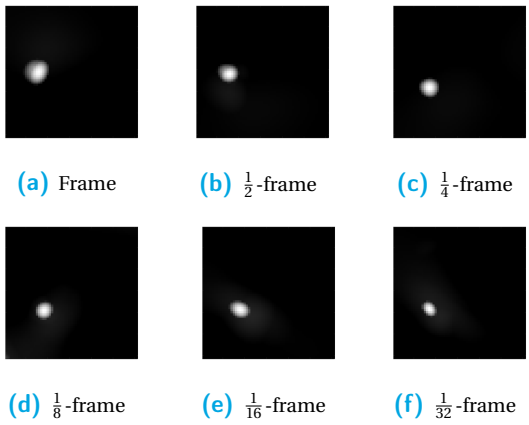

Figure 8: Reconstructed dynamic images from noisy simulated data in the fast scenario where different sizes of subproblems are considered within the RESESOP-Kaczmarz algorithm.

native approach based on prior reconstruction discussed in Section II.III.1.

Figure 6 illustrates the influence of different inexactness levels on the reconstruction result of RESESOP-Kaczmarz. Both the proposed norm estimation directly from the measured data as well as the estimation from prior static reconstructions with regularized Kaczmarz result in images of similar quality (unless in the underestimated case, see first row, where the computation from the data is beneficial). Nevertheless, an underestimation of the inexactness levels leads to an increase in motion artifacts, while the motion is well compensated for even if largely overestimated levels are used. The algorithm is also stable regarding (random) errors in the computed inexactness levels, see column 2. Despite strong deviations of overall 15%, the algorithm still provides a reconstruction of comparable image quality as with the exact values.

Next, we study how the reconstruction quality develops in dependence on the number of iterations. As was shown in [16], the algorithm converges monotone as long as adequate search directions are chosen. This is clearly visible in Figure 7 which shows the evolution of the NRMSE of the RESESOP-Kaczmarz solution compared to the ground truth with increasing number of iterations. Furthermore, we observe that the error reduces rapidly during the first iteration and then flattens out.

Lastly, we want to examine the influence of the size of the subproblems. Depending on the speed of the motion, assuming the concentration to be static during a complete Lissajous trajectory can be too much simplified. Indeed, Figure 4 shows that under this assumption in the very fast scenario, the reconstructed object is not correctly located. This can be improved by considering subproblems of smaller size, see Figure 8.

Choosing the sizes of the subproblems as a quarter of a frame or smaller improves the reconstructed location of the object, see e.g. Figure 8c. However, choosing the size too small can reintroduce a low amount of noise in the reconstruction, see Figures 8e and 8f. Thus, in case of very fast motion, one has to balance motion compensation and noise reduction when choosing appropriate sizes of subproblems.

IV.III. Real Data

In this section we evaluate the performance of RESESOP-Kaczmarz on the real data introduced in Section III.II.

Figure 9 depicts reconstructions of four consecutive frames of real data. For both the fullframe and subframe scenarios, the pre-processing steps described in Section III.III were applied. The left column shows images computed with RESESOP-Kaczmarz using frame-sized subproblems. From the reconstructed images, we can clearly deduce the temporal evolution of the object, namely the rotation of the glass capillary. Also its spatial location per time step is overall well captured and the noise well suppressed. However, examining frames one, two and four the circular shape of the reconstructed glass capillary is slightly distorted due to the fast motion.

The right column of Figure 9 shows the respective reconstruction results using $\frac{1}{4}$-frames as subproblems. Compared to the frame-wise case, they portray the object with a more constant round shape but are also more affected by noise. This illustrates again the trade-off between noise reduction and motion compensation. In a future step, it would be interesting to study whether algorithms (or reconstructions) for different subproblem sizes could be merged in order to combine the good motion compensation property of small subproblems with the better noise reduction of large subproblems.

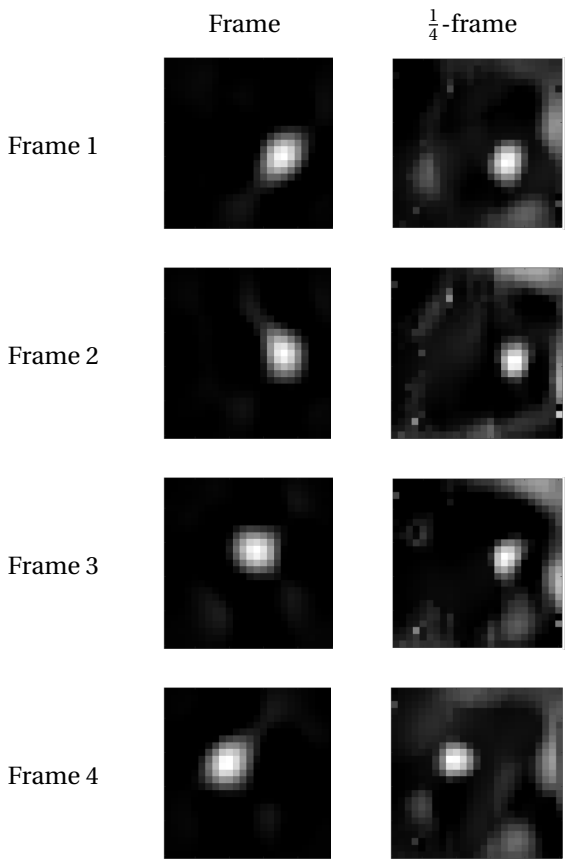

Figure 9: Reconstructed dynamic image sequence with RESESOP-Kaczmarz of four consecutive frames of real data for a 7 Hz rotation with different sized subproblems. The first subframe per frame is depicted. The original numeration of the frames starts at frame 750.

V. Conclusion

In this article, we propose the RESESOP-Kaczmarz algorithm to reconstruct dynamic objects from MPI data. The method takes motion into account as a model inexactness and, within the MPI framework, the only required a priori information can be computed directly from the measured data. The potential of the method was demonstrated on real and simulated data. In particular, our detailed experiments on simulated data show the robustness of the method regarding its various parameters and that it outperforms the regularized Kaczmarz algorithm, a common solver in MPI based on a stationary assumption on the object. Since the method further allows to consider subproblems smaller than one complete frame, it is suitable for a variety of dynamic MPI problems, including scenarios with rapid particle movements.

Acknowledgments

The authors acknowledge the support by 'Deutsche Forschungsgemeinschaft' under grant HA 8176/2-1. The authors further thank Hannes Albers and Tobias Kluth for providing us with simulated data as well as Christina Brandt and Tobias Knopp for real data.

References

[1] B. Gleich and J. Weizenecker. Tomographic imaging using the nonlinear response of magnetic particles. *Nature*, 435(7046):1214–1217, 2005, doi:10.1038/nature03808.

[2] T. Knopp and T. M. Buzug, Magnetic Particle Imaging: An Introduction to Imaging Principles and Scanner Instrumentation. Berlin, Heidelberg: Springer Berlin Heidelberg, 2012, doi:10.1007/978-3-642-04199-0.

[3] H. Albers, T. Knopp, M. Möddel, M. Boberg, and T. Kluth. Modeling the magnetization dynamics for large ensembles of immobilized magnetic nanoparticles in multi-dimensional magnetic particle imaging. *Journal of Magnetism and Magnetic Materials*, 543:168534, 2022, doi:10.1016/j.jmmm.2021.168534.

[4] M. Nitzsche, H. Albers, T. Kluth, and B. Hahn. Compensating model imperfections during image reconstruction via Resesop. *International Journal on Magnetic Particle Imaging*, 8(1 Suppl. 1), 2022, doi:10.18416/IJMPI.2022.2203062.

[5] J. Weizenecker, B. Gleich, J. Rahmer, H. Dahnke, and J. Borgert. Three-dimensional real-time in vivo magnetic particle imaging. *Physics in Medicine and Biology*, 54(5):L1–L10, 2009, doi:10.1088/0031-9155/54/5/L01.

[6] J. Haegele, J. Rahmer, B. Gleich, J. Borgert, H. Wojtczyk, N. Panagiotopoulos, T. M. Buzug, J. Barkhausen, and F. M. Vogt. Magnetic Particle Imaging: Visualization of Instruments for Cardiovascular Intervention. *Radiology*, 265(3):933–938, 2012, doi:10.1148/radiol.12120424.

[7] M. Graeser, F. Thieben, P. Szwargulski, F. Werner, N. Gdaniec, M. Boberg, F. Griese, M. Möddel, P. Ludewig, D. van de Ven, O. M. Weber, O. Woywode, B. Gleich, and T. Knopp. Human-sized magnetic particle imaging for brain applications. *Nature Communications*, 10(1):1936, 2019, doi:10.1038/s41467-019-09704-x.

[8] P. Ludewig, M. Graeser, N. D. Forkert, F. Thieben, J. Rández-Garbayo, J. Rieckhoff, K. Lessmann, F. Förger, P. Szwargulski, T. Magnus, and T. Knopp. Magnetic particle imaging for assessment of cerebral perfusion and ischemia. *WIREs Nanomedicine and Nanobiotechnology*, 14(1), 2022, doi:10.1002/wnan.1757.

[9] N. Gdaniec, M. Schluter, M. Moddel, M. G. Kaul, K. M. Krishnan, A. Schlaefer, and T. Knopp. Detection and Compensation of Periodic Motion in Magnetic Particle Imaging. *IEEE Transactions on Medical Imaging*, 36(7):1511–1521, 2017, doi:10.1109/TMI.2017.2666740.

[10] N. Gdaniec, M. Boberg, M. Moddel, P. Szwargulski, and T. Knopp. Suppression of Motion Artifacts Caused by Temporally Recurring Tracer Distributions in Multi-Patch Magnetic Particle Imaging. *IEEE Transactions on Medical Imaging*, 39(11):3548–3558, 2020, doi:10.1109/TMI.2020.2998910.

[11] C. Brandt and C. Schmidt. Modeling Magnetic Particle Imaging for Dynamic Tracer Distributions. *Sensing and Imaging*, 22(1):45, 2021, doi:10.1007/s11220-021-00368-w.

[12] C. Brandt and C. Schmidt. Motion compensation for non-periodic dynamic tracer distributions in multi-patch magnetic particle imaging. *Physics in Medicine & Biology*, 67(8):085005, 2022, doi:10.1088/1361-6560/ac5ce6.

[13] M. Burger, H. Dirks, and L. Frerking, 7. On optical flow models for variational motion estimation, in *Variational Methods*, De Gruyter, 2016, 225–251. doi:10.1515/9783110430394-007.

[14] T. Kluth, B. Hahn, and C. Brandt, Spatio-temporal concentration reconstruction using motion priors in magnetic particle imaging, in *International Workshop on Magnetic Particle Imaging*, 2019.

[15] C. Brandt, T. Kluth, T. Knopp, and L. Westen. Dynamic image reconstruction with motion priors in application to 3D magnetic particle imaging, 2023. arXiv: 2306.11625. URL: http://arxiv.org/abs/2306.11625.

[16] S. E. Blanke, B. N. Hahn, and A. Wald. Inverse problems with inexact forward operator: iterative regularization and application in dynamic imaging. *Inverse Problems*, 36(12):124001, 2020, doi:10.1088/1361-6420/abb5e1.

[17] M. G. Kaul, J. Salamon, T. Knopp, H. Ittrich, G. Adam, H. Weller, and C. Jung. Magnetic particle imaging for in vivo blood flow velocity measurements in mice. *Physics in Medicine & Biology*, 63(6):064001, 2018, doi:10.1088/1361-6560/aab136.

[18] B. N. Hahn. Efficient algorithms for linear dynamic inverse problems with known motion. *Inverse Problems*, 30(3):035008, 2014, doi:10.1088/0266-5611/30/3/035008.

[19] L. Desbat, S. Roux, and P. Grangeat. Compensation of Some Time Dependent Deformations in Tomography. *IEEE Transactions on Medical Imaging*, 26(2):261–269, 2007, doi:10.1109/TMI.2006.889743.

[20] F. Schöpfer, T. Schuster, and A. K. Louis. Metric and Bregman projections onto affine subspaces and their computation via sequential subspace optimization methods. *JIIP*, 16(5):479–506, 2008, doi:10.1515/JIIP.2008.026.

[21] F. Schöpfer and T. Schuster. Fast regularizing sequential subspace optimization in Banach spaces. *Inverse Problems*, 25(1):015013, 2009, doi:10.1088/0266-5611/25/1/015013.

[22] T. Kluth, P. Szwargulski, and T. Knopp. Towards accurate modeling of the multidimensional magnetic particle imaging physics. *New Journal of Physics*, 21(10):103032, 2019, doi:10.1088/1367-2630/ab4938.

[23] H. Albers, T. Kluth, and T. Knopp. Simulating magnetization dynamics of large ensembles of single domain nanoparticles: Numerical study of Brown/Néel dynamics and parameter identification problems in magnetic particle imaging. *Journal of Magnetism and Magnetic Materials*, 541:168508, 2022, doi:10.1016/j.jmmm.2021.168508.

[24] T. Kluth and B. Jin. Enhanced reconstruction in magnetic particle imaging by whitening and randomized SVD approximation. *Physics in Medicine & Biology*, 64(12):125026, 2019, doi:10.1088/1361-6560/ab1a4f.

